Düzce University Journal of Science & Technology

Research Article

Effect of Different Dimpled Fin Configurations and Angles on Entropy Generation, Flow Behavior, and Thermal Performance

Emrehan GÜRSOY [a,*], Alper ERGÜN [b], Engin GEDİK [b]

[a] *Audit Department, Kardemir Karabük Iron Steel Industry Trade & Co. Inc., Karabük, TÜRKİYE*
[b] *Department of Mechanical Engineering, Faculty of Engineering, Karabük University, Karabük, TÜRKİYE*
* *Corresponding author's e-mail address: emrehangursoy@gmail.com*
DOI: 10.29130/dubited.1473175

ABSTRACT

Recent studies highlight that flow in tubes with dimpled fins provides significant thermal performance improvement. Although the variety of these fins comes to the fore today, there is no comprehensive study on which geometry provides better performance. In this study, the heat transfer, entropy generation, and performance effects of dimpled fins with 6 different geometries and 17 different configurations, machined on a smooth tube and having the same surface area, were numerically analysed under steady-state, thermally and hydrodynamically developing flow conditions. Water has been considered as working fluid and it flowed under laminar conditions (1000≤Re≤2000). According to obtained results, the cube-shaped dimpled fins arranged as parallel to flow (CuDT/C) exhibit the highest average Nusselt number, with increases of 95.21%, 176.25%, and 272.13% for Re=1000, 1500, and 2000, respectively, compared to smoot tube. It has been determined that CuDT/C increases the performance evaluation criterion at the rates of 65.94%, 115.96%, and 176.79% for Re=1000, 1500, and 2000, respectively.

Keywords: *Different dimpled fin types, Entropy generation, Laminar flow regime, Performance evaluation criterion, Thermo-hydraulic performance*

Farklı Çukurlu Kanat Konfigürasyonları ve Açılarının Entropi Üretimi, Akış Davranışları ve Termal Performans Üzerindeki Etkisi

ÖZ

Son yapılan çalışmalar, çukurlu kanatçıklara sahip kanallardaki akışın önemli ölçüde termal performans iyileştirmesi sağladığını vurgulamaktadır. Ancak günümüzde bu kanat çeşitliliği öne çıkmasına rağmen, hangi geometrinin daha iyi performans sağladığına dair kapsamlı bir çalışma bulunmamaktadır. Bu çalışmada, düz boru üzerinde işlenmiş ve aynı yüzey alanına sahip 6 farklı geometri ve 17 farklı konfigürasyonuna sahip çukur kanatların, ısı transferi, entropi üretimi ve performans etkileri, sürekli durum, ısıl ve hidrodinamik olarak gelişen akış koşullarında sayısal olarak analiz edilmiştir. Çalışma akışkanının su olduğu ve laminer koşullar altında (1000≤Re≤2000) akışın gerçekleştiği varsayılmıştır. Elde edilen sonuçlara göre akışa paralel olarak düzenlenmiş küp şekilli çukur kanatlar (CuDT/C), en yüksek ortalama Nusselt sayısını sağlamıştır ve düz kanal ile kıyaslandığında Re=1000, 1500 ve 2000 için sırasıyla %95,21, %176,25 ve %272,13 artışlar kaydedilmiştir. CuDT/C'nin performans değerlendirme kriterini Re=1000, 1500 ve 2000 için sırasıyla %65,94, %115,96 ve %176,79 oranlarında artırdığı belirlenmiştir.

Anahtar Kelimeler: *Entropi üretimi, Farklı çukur kanat tipleri, Laminer akış rejimi, Performans değerlendirme katsayısı, Termo-hidrolik performans.*

Received: 24/04/2013, Revised: 01/05/2024, Accepted: 21/05/2024

I. INTRODUCTION

Heat transfer enhancement studies have gained importance due to the increase in energy consumption on a global scale and the decrease energy sources [1]. As a result, researchers and engineers have proposed many methods grouped under two main heat transfer enhancement techniques passive and active [2]. From a different viewpoint, passive heat transfer enhancement techniques are preferred over active heat transfer enhancement techniques because of their simple producibility and cost-effectiveness during both operation and investment [3]. Therefore, most researchers have spent their time examining the heat transfer and flow characteristics of passive heat transfer enhancement techniques [4], [5].

According to previous studies, dimpled fins evaluated under heat transfer area augmentation procure an important enhancement rate and control compared with others [4]. On the basis of this outcome, many researchers have carried out remarkable studies both experimentally and numerically. It is aimed to reveal the heat transfer phenomenon of dimpled fin shapes and rheological functions in these studies. For example, Paul et al. [6] conducted a numerical study on a cross-flow heat exchanger modelled with spherical dimpled fins. The results show that dimpled fins enhanced the Nusselt number (Nu) at the rate of 7.33% compared to smooth surfaces. Besides, the maximum performance evaluation criterion (PEC) has been found as 1.034 on the condition using the dimpled fins. Pazarlıoğlu et al. [7] conducted a detailed study on a sudden expansion tube modified with elliptical dimpled fins under a laminar flow regime. In the study, dimpled fins were aligned in different positions, horizontal and vertical. According to the results, vertically aligned dimpled fins performed remarkable increments in convective heat transfer compared with horizontal fins. Another special dimpled fin-shaped study was performed by Zhang and colleagues [8]. They used star-shaped dimpled fins locally mounted on a tube to examine the heat transfer and flow characteristics. The result indicated that star-shaped dimpled fins performed a more convective heat transfer than elliptical dimpled fins at a rate of 24.8%. Sabir et al. [9] numerically investigated the thermo-hydraulic performance of both elliptical and teardrop dimpled fins under a turbulent flow regime with a range of 9000≤Reynolds number (Re)≤40000. The researchers have determined the optimal working range in their study. Another performance enhancement investigation for a teardrop-dimpled tube on twisted tape was conducted by Bucak and Yılmaz [10]. The simulations were conducted for 3000≤Re≤27000 and different pattern densities (N=30 and 45). The results demonstrated that teardrop dimpled fins can increase the thermal performance by up to 50%. Mironov et al. [11] performed a numerical analysis on a tube retrofitted with capsule dimpled fins, which have different geometric configurations, to examine the heat transfer performance, vortex generation, and flow characteristics of a heat exchanger. According to the results, it can be seen that not only does the application of oval dimpled fins increase the convective heat transfer rate in the system, but also the change in the oval shape significantly affects this phenomenon.

Based on existing studies, many researchers have carried out many studies on different fin shapes to reveal the thermo-hydraulic performance of the system. However, there is no comprehensive study aimed at determining which fin shape is prominent in terms of thermo-hydraulic performance and entropy generation on a thermal system. For this purpose, a comparative study was conducted on six different dimpled fins, including different placement angles, in the scope of this study. In total, seventeen geometries have been investigated independently from the surface area under laminar flow conditions (1000≤Re≤2000). The results are comparatively given and supported by several contours and local velocity vectors.

II. MATERIAL METHOD

Detailed information about numerical analysis, working fluid, and solution methods has been presented in this section.

A. DESCRIPTION OF THE ANALYSIS DATA

In this numerical study, a comparative investigation was conducted to present the thermo-hydraulic characteristics of different dimpled fin shapes with different placement angles. Summarized geometric information, dimensions of the dimpled fins, and boundary conditions are presented in Figure 1. As the fluid domain, a circular tube with length and diameter L=1500 mm and D=16 mm was used, respectively, and water has been used as a working fluid at Re=1000, 1500, and 2000. In addition, the fluid enters the tube at a constant inlet temperature of 300 K and as a hydrodynamically developing flow. Different dimpled fins with $A_{surface}$= 36 mm^2 were mounted on the tube at a pitch length of P=15 mm, and the entire wall was heated by an imaginary heater by exposure to a heat flux of q″=600 W/m^2. The inlet velocity (V_{inlet}) shows variation with Re, and it has been assumed that fluid flows to the atmosphere (P_{outlet}=1 atm). Several assumptions given below have been considered in this study.

- Solutions are conducted for single-phase,
- The no-slip condition is accepted for the entire tube wall,
- Buoyancy force and inertial force are neglected,
- Fluid flow is incompressible,

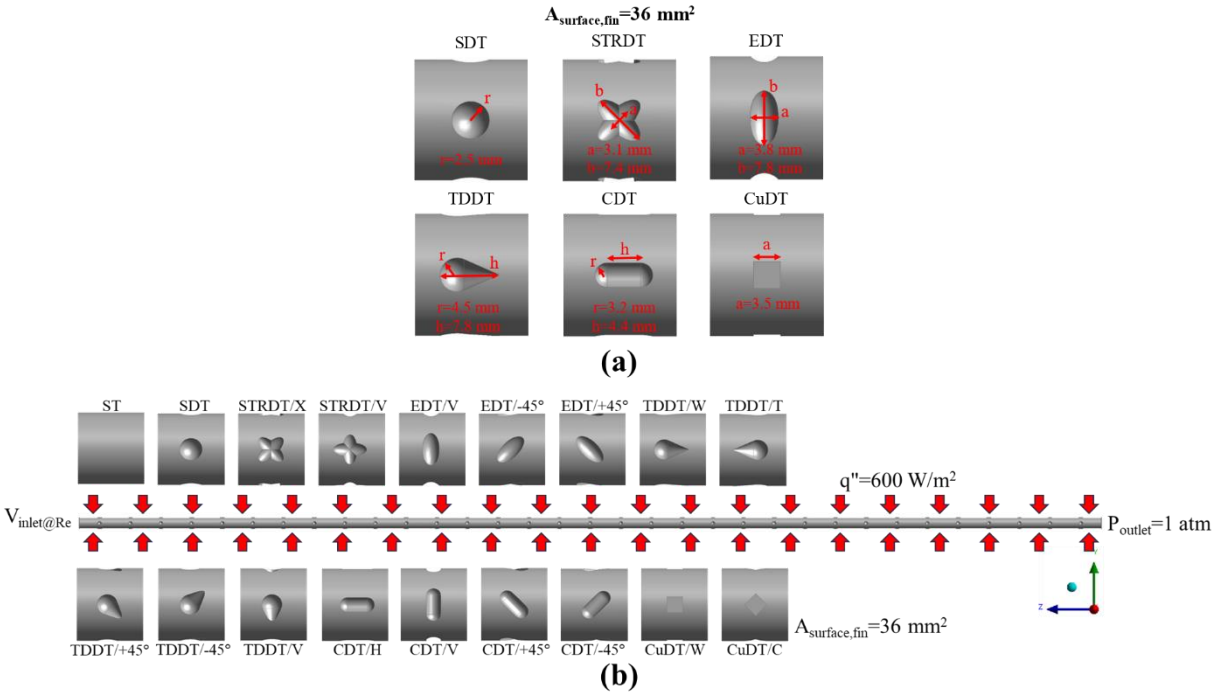

Figure 1. *Detailed view of;* ***(a)*** *dimpled fin dimensions and* ***(b)*** *boundary conditions of the computed fluid domain.*

B. GOVERNING EQUATIONS

Based on the assumption given in the above section, the dimensionless governing equations are as follow:

Continuity equation [12]:

$$\frac{\partial U_x}{\partial x}+\frac{\partial U_y}{\partial y}+\frac{\partial U_z}{\partial z}=0 \tag{1}$$

Momentum equation [12]:

$$\frac{\partial (U_i U_x)}{\partial x}+\frac{\partial \left(U_i U_y\right)}{\partial y}+\frac{\partial (U_i U_z)}{\partial z}=-\frac{\partial p}{\partial i}+\frac{1}{Re}\left(\frac{\partial \tau_{xi}}{\partial x}+\frac{\partial \tau_{yi}}{\partial y}+\frac{\partial \tau_{zi}}{\partial z}\right) \tag{2}$$

Energy equation [12]:

$$\frac{\partial(U_x T)}{\partial x}+\frac{\partial\left(U_y T\right)}{\partial y}+\frac{\partial(U_z T)}{\partial z}=\frac{1}{RePr}\left(\frac{\partial^2 T}{\partial x^2}+\frac{\partial^2 T}{\partial y^2}+\frac{\partial^2 T}{\partial z^2}\right) \quad (3)$$

C. DATA REDUCTION

Some dimensionless and mathematical impressions were used in the study to reach meaningful results in terms of heat transfer and flow characteristics. In this connection, Re, which is a dimensionless flow regime indicator, has been used to determine the flow regime status as given in Eq. (4) [13].

$$Re=\frac{\rho U D}{\mu} \quad (4)$$

where, ρ [kg/m^3], U [m/s], D [m], and μ [kg/ms] specify the density, velocity, diameter, and dynamic viscosity, respectively. When considering the adiabatic mixing of the working fluid in the tube, the equilibrium temperature defined as the bulk temperature can be found in Eq. (5). In addition, the convective heat transfer rate between the tube wall and the working fluid can be identified with Eq. (6) [13].

$$T_b=\frac{T_{inlet}+T_{outlet}}{2} \quad (5)$$

$$h=\frac{q^{"}}{T_w-T_b} \quad (6)$$

where, q″ [W/m^2] and T_w [K] describe the heat flux and average wall temperature, respectively. Furthermore, dimensionless convective heat transfer can be expressed using Eq. (7) [14].

$$Nu=\frac{hD}{k} \quad (7)$$

where, k [W/mK] is the thermal conductivity of the working fluid. To determine the frictional energy loss through the longitudinal tube, the theoretical Darcy friction factor given in Eq. (8) can be used [14].

$$ff=\frac{\Delta P}{\frac{L}{D}\frac{\rho V^2}{2}} \quad (8)$$

where ΔP [Pa] denotes the pressure drop between the inlet and outlet of the tube. In addition, PEC, which is a dimensionless number, is used to reveal the effectiveness of the dimpled fins and can be calculated with Eq. (9) [15]. In this equation, Nu and ff obtained from a dimpled tube (DT) are compared to those from a smooth tube (ST), and the cases provided with a PEC>1 condition are considered.

$$PEC=\frac{Nu_{xDT}/Nu_{ST}}{f_{xDT}/f_{ST}} \quad (9)$$

Another investigation of thermal system performance examines entropy generation. In thermal systems, considerable irreversibility occurs due to friction, finite temperature differences, and chemical reaction phenomena. Thanks to this, the entropy generation effect of different dimpled fins has been investigated. The total entropy generation is divided into two sections: thermal entropy generation and frictional entropy generation arising from finite temperature difference and friction along the tube, respectively. The equations related to entropy generation are presented in Eqs. (10)-(12) [7].

$$\dot{S}_{gen,total} = \dot{S}_{gen,thermal} + \dot{S}_{gen,frictional} \quad (10)$$

$$\dot{S}_{gen,thermal} = \frac{q'^2 L}{\pi k Nu T_b^2} \quad (11)$$

$$\dot{S}_{gen,frictional} = \frac{32\dot{m}^3 f L}{\rho^3 T_b \pi^2 D^5} \quad (12)$$

where, q´ [W/m] specifies the applied heat power magnitude per meter. On the other hand, the Bejan number (Be), which evaluates the share of thermal entropy generation on total entropy generation, has been researched via Eq. (13) [7].

$$Be = \frac{\dot{S}_{gen,thermal}}{\dot{S}_{gen,total}} \quad (13)$$

D. THERMOPHYSICAL PROPERTIES OF THE WORKING FLUID

Water, which is one of the most used heat trasnfer fluids in systems, was selected as the working fluid in this study. The thermophysical properties of water are shown in Table 1.

Table 1. *Thermophysical properties of water [16].*

Thermophysical Properties	Magnitude
Density, ρ, kg/m^3	998.2
Thermal Conductivity, k, W/mK	0.6
Specific Heat, cp, J/kgK	4182.0
Dynamic Viscosity, μ, kg/ms	0.001003

E. COMPUTATIONAL SOLUTION PROCEDURE

In this numerical investigation, the steady state and single-phase solution approach was employed. The analysis focused on laminar flow conditions, encompassing activities such as geometry formation, mesh examination, solution processing, and post-processing using the ANSYS Fluent 2020 R2 software. Computational data were processed using the pressure-based type and absolute velocity formulation, with the SIMPLE algorithm for pressure-velocity coupling. The second-order upwind scheme was deliberately chosen because its ability to ensure reasonable stability in internal flow issues across all simulations. Error minimization in the analyses was achieved by adopting of the least squares cell-based method. Meanwhile, the iterative process persisted until the residuals reached a threshold of 10^{-6}.

F. MESH CONVERGENCE STUDY AND MESH STRUCTURE

Since the numerical analyses were carried out according to the Finite Volume Method, the fluid domain was divided into many small volumes, and software conducted the analysis process for each small volume. When dividing the fluid domain into small volumes, attention should be paid to mesh quality values and mesh methods. In this study, local and general mesh settings were used to form the mesh structure, and a tetrahedron mesh structure was used. In each mesh setting obtained, skewness and orthogonal mesh quality values were considered. Since the number of mesh structures formed in the fluid domain directly affects the results and solution time, a mesh independence study was conducted. The relevant study was performed for the case where water at Re=2000 flows from the ST. According to the outcomes of this study, variations in the results, number of meshes, and quality values are given in Table 2. The mesh structures belonging to ST and CuDT/C taken from selected mesh settings are shown in Figure 2.

Table 2. *Mesh convergence study results.*

Study No	Mesh Number	Nu	Deviation of Nu	f	Deviation of f	Min. Orthogonal Quality	Max. Skewness Quality
1	52360	11.20	19.79%	0.0372	9.4%	0.564	0.725
2	220540	10.54	12.73%	0.0345	2.2%	0.611	0.605
3 (selected)	425600	9.39	0.43%	0.0339	0.5%	0.815	0.469
4	621560	9.36	0.11%	0.0338	0.3%	0.841	0.415
5	740400	9.35	0.0%	0.0338	0.3%	0.865	0.406
6	950390	9.35	0.0%	0.0337	0.0%	0.894	0.401

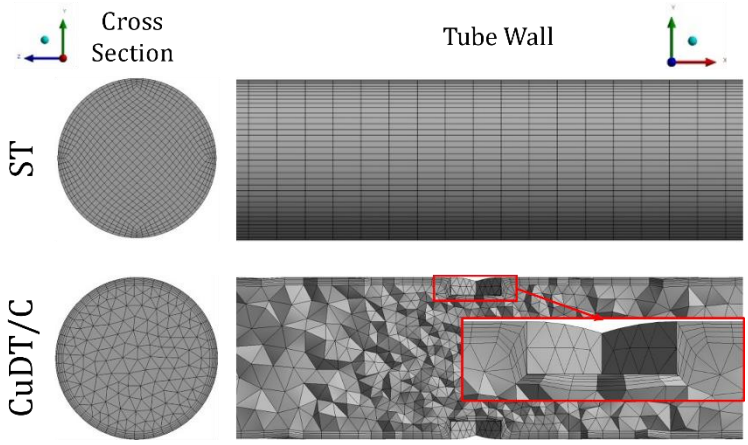

Figure 2. *The mesh structure of ST and CuDT/C after optimal settings.*

III. RESULTS

Before the start of continuous analyses, validation of the mesh structures and solution procedures has to be performed. For this purpose, the validation process of the fluid domain has been conducted for ST using water at Re=1000, 1500, and 2000, and well-known correlations in the literature were used for comparison. Whereas Shah-London and Sieder-Tate correlations, which are given for the laminar flow regime, have been used for the validation of Nu, Hagen–Poiseuille has been utilized for the validation of ff. These equations and auxiliary equations have been presented in Eqs. (14)-(17), respectively. The comparative results are presented in Figure 3. According to the results, the error rate of Nu has been detected as 4.72% and 9.76% at Re=2000 compared to Sieder-Tate and Shah-London correlations, respectively. Besides, the error rate of ff has been found to be 5.71% compared to the Hagen-Poiseuille correlation. Generally, the obtained error rate can be accepted for continuous analyses when looking at published studies.

Shah-London correlation [17]:

$$Nu = 1.953\left(Re \cdot Pr.\frac{D}{L}\right)^{1/3};\ \left(Re \cdot Pr.\frac{D}{L}\right) \geq 33.3 \tag{14}$$

Sieder-Tate correlation [18]:

$$Nu = 1.86\left(Re \cdot Pr.\frac{D}{L}\right)^{1/3} \tag{15}$$

Hagen- Poiseuille correlation [19]:

$$ff = \frac{64}{Re} \tag{16}$$

Prandtl number [20]:

$$Pr = \frac{c_p \mu}{k} \tag{17}$$

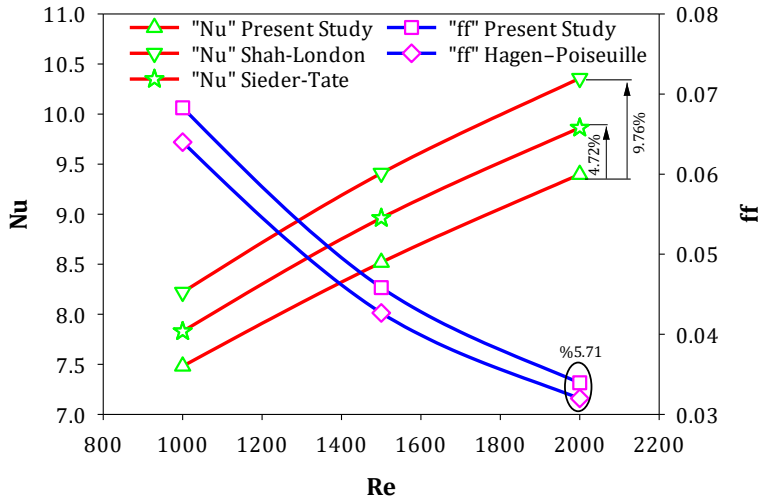

Figure 3. *Validation of the numerical results with well-known correlations.*

The convective heat transfer performance of DTs has been presented in Figure 4 as a function of Re. The results show that as Re increases, Nu tends to increase as expected. The highest Nu has been obtained from the CuDT/C case as 34.97 at Re=2000. The main reason for these results is based on the effect of the cube shape and its placement angle on flow characteristics. As the working fluid flows over the CuDT/C, it divides into two and forms the highest vortex in the channel as shown in Figure 12. This contributes to the hydraulic boundary layer on the near-wall being distributed and heat transfer being increased. The order of the cases from highest to lowest at Re=2000 according to Nu is as follows; CuDT/C, SDT, CuDT/W, TDDT/-45°, TDDT/+45°, TDDT/W, TDDT/V, TDDT/T, CDT/+45°, CDT/V, CDT/-45°, EDT/+45°, EDT/-45°, EDT/V, STRDT/V, CDT/H, STRDT/X, ST. Besides, the Nu increment rate of CuDT/CT is acquired as 95.21%, 176.25%, and 272.13% at Re=1000, 1500, and 2000, respectively. Furthermore, the placement angle transition of CuDT from W to C resulted in enhancement of 26.47%, 51.54%, and 65.46% at Re=1000, 1500, and 2000, respectively.

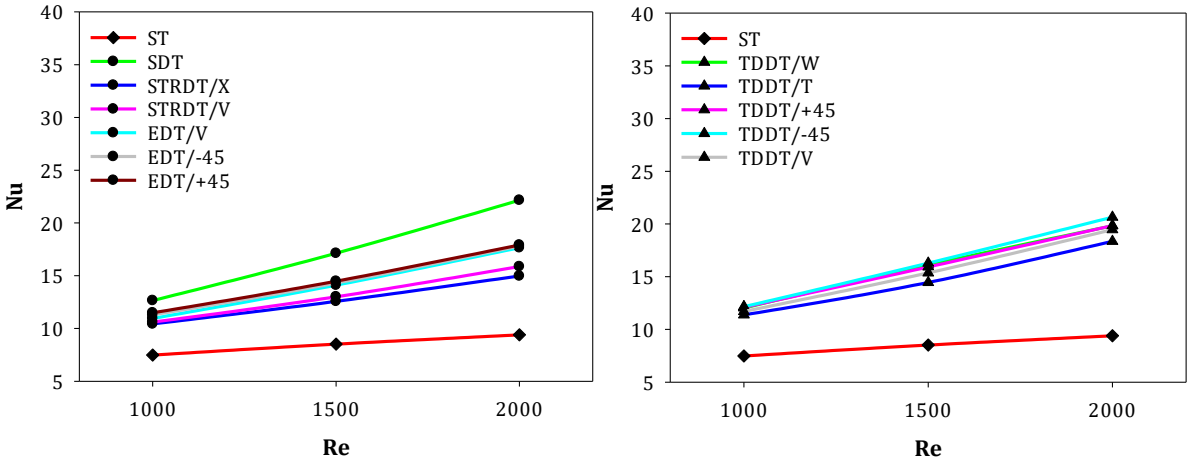

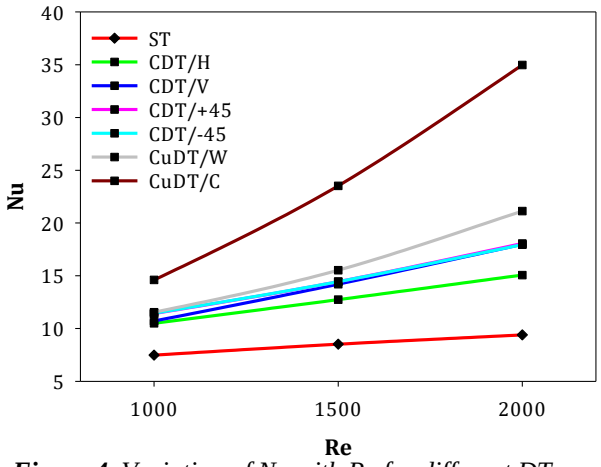

Figure 4. *Variation of Nu with Re for different DTs.*

Variation of ff with Re is given in Figure 5. The results show that as Re increases, ff tends to decrease as expected. The lowest ff has been presented by CDT/H, except for ST. The increment rate of ff along with CFT/H is realized as 37.35%, 51.37%, and 66.90% for Re=1000, 1500, and 2000, respectively. The order of the cases from lowest to highest at Re=2000 according to ff is as follows; ST, CDT/H, STRDT/X, STRDT/V, TDDT/T, TDDT/W, CDT/V, CDT/-45, CDT/+45, EDT/-45, CuDT/W, TDDT/+45, EDT/+45, EDT/V, TDDT/-45, TDDT/V, SDT, CuDT/C. Besides, the placement angle transition of CDT from H to V, +45°, and -45° causes a decrease of 15.16%, 16.19%, and 16.31% at Re=2000, respectively.

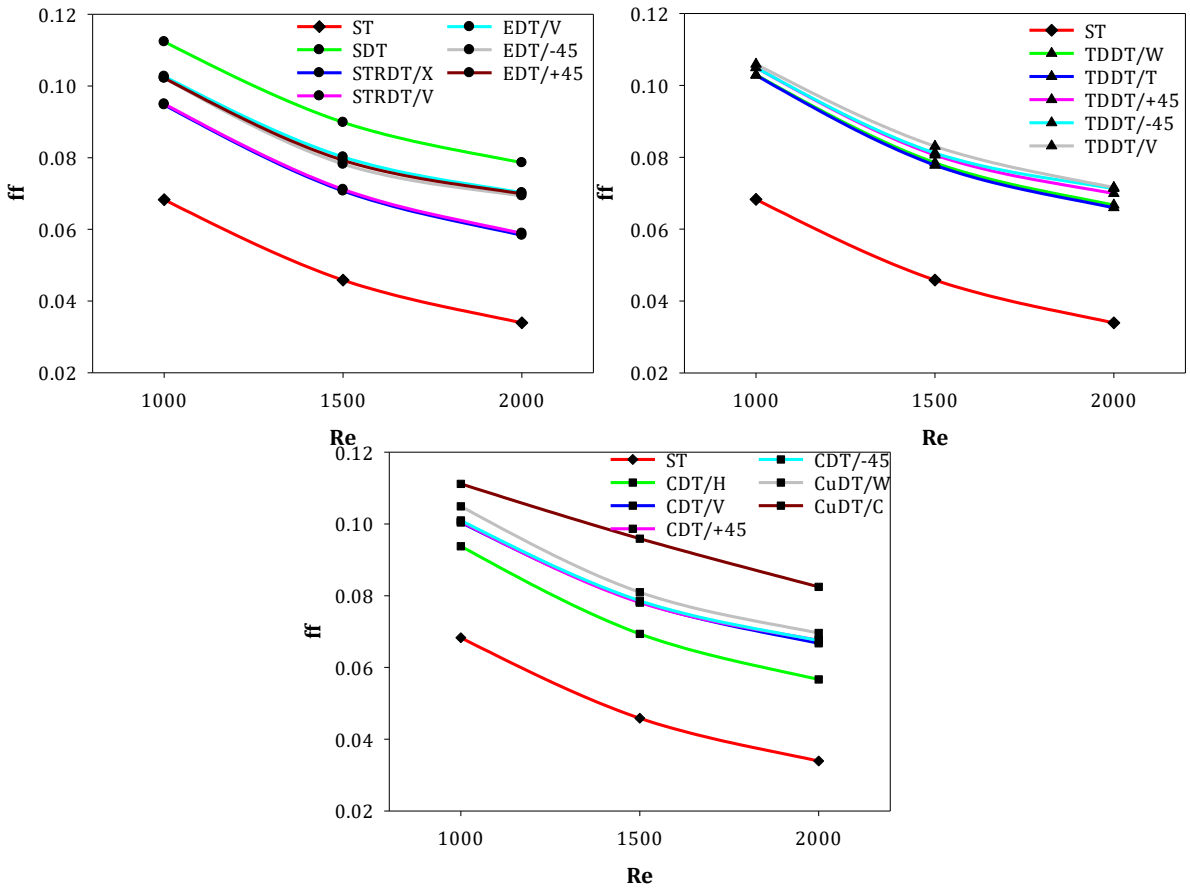

Figure 5. Variation of ff with Re for different DTs.

Based on the Nu and ff results, the PEC, which shows the effectiveness factor of enhancement techniques, is presented in Figure 6 as a function of Re. The results indicate that although CuDT/C causes the highest ff among the fin types, it performed the highest PEC. The reason for this result is that CuDT/C forms more vortices, distributing the velocity and temperature boundary layers and causing Nu to be more dominant on f. According to the calculation, CuDT/C increases the PEC at the rates of 65.94%, 115.96%, and 176.79% for Re=1000, 1500, and 2000, respectively. Compared to CuDT/W, the PEC results of CuDT/C exhibited an increase of 19.39%, 30.18%, and 36.05% at Re=1000, 1500, and 2000, respectively.

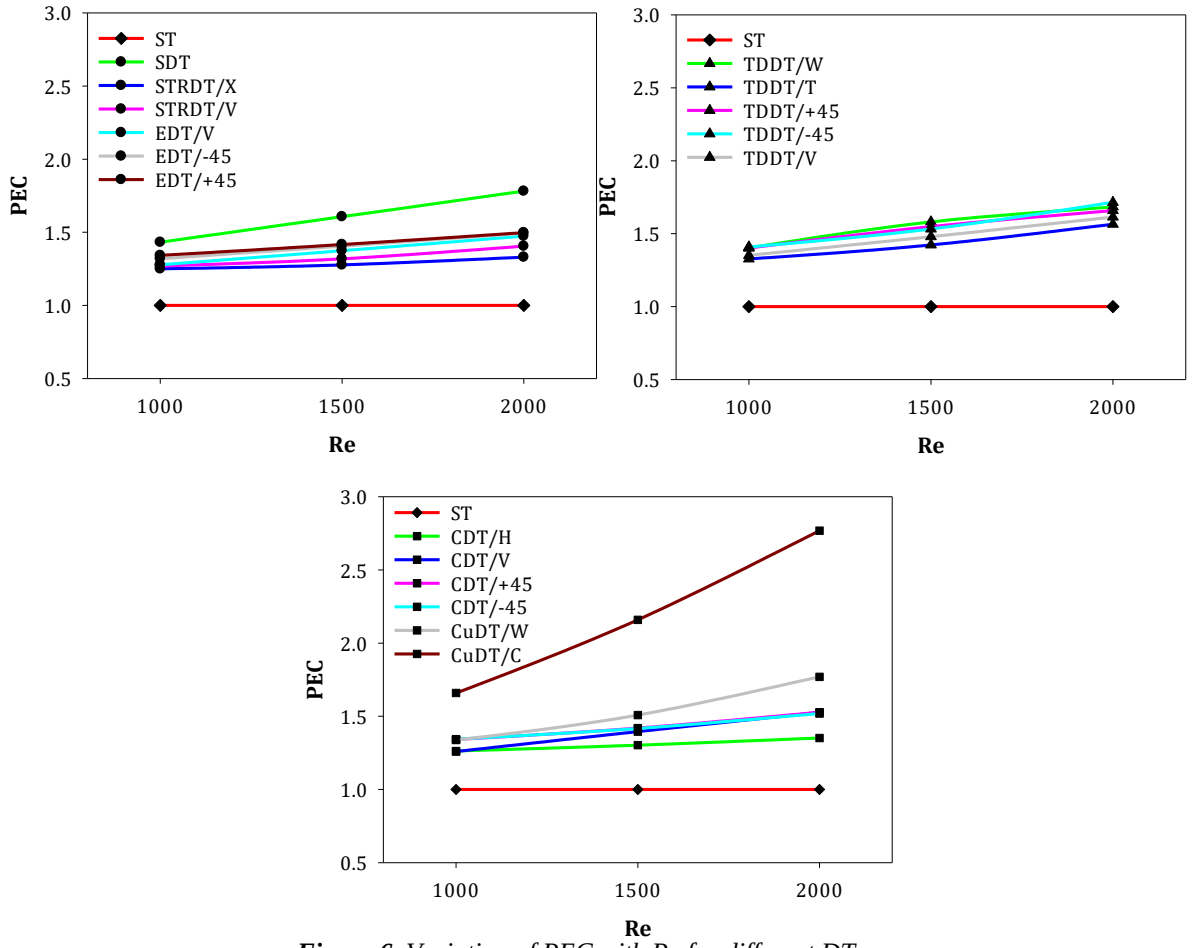

Figure 6. *Variation of PEC with Re for different DTs.*

The entropy generation arising from the finite temperature difference is presented in Figure 7 for all DTs. According to the result, all DTs show a remarkable decrease in $\dot{S}_{gen,\ thermal}$ compared to ST and the lowest situation has been performed by CuDT/C. The decrement rate in CuDT/C has been realized as 40.49%, 54.36%, and 63.37% for Re=1000, 1500, and 2000, respectively, compared to ST. When investigating the dimpled fin placement angle effect on $\dot{S}_{gen,\ thermal}$, CuDT/C provided a decrease of 17.56%, 27.83%, and 30.63% compared with CuDT/W. The reason for this is that CuDT/C forms more vorticity on both the upstream side and around, with this effect becoming more pronounced as Re increases. This vorticity positively affects the thermal and hydrodynamic boundary layers, enhancing the fluid's ability to absorb heat from the heated surface of the tube, thereby increasing convective heat transfer. Because of this, $\dot{S}_{gen,\ thermal}$ performed more decreasing with the help of CuDT/C.

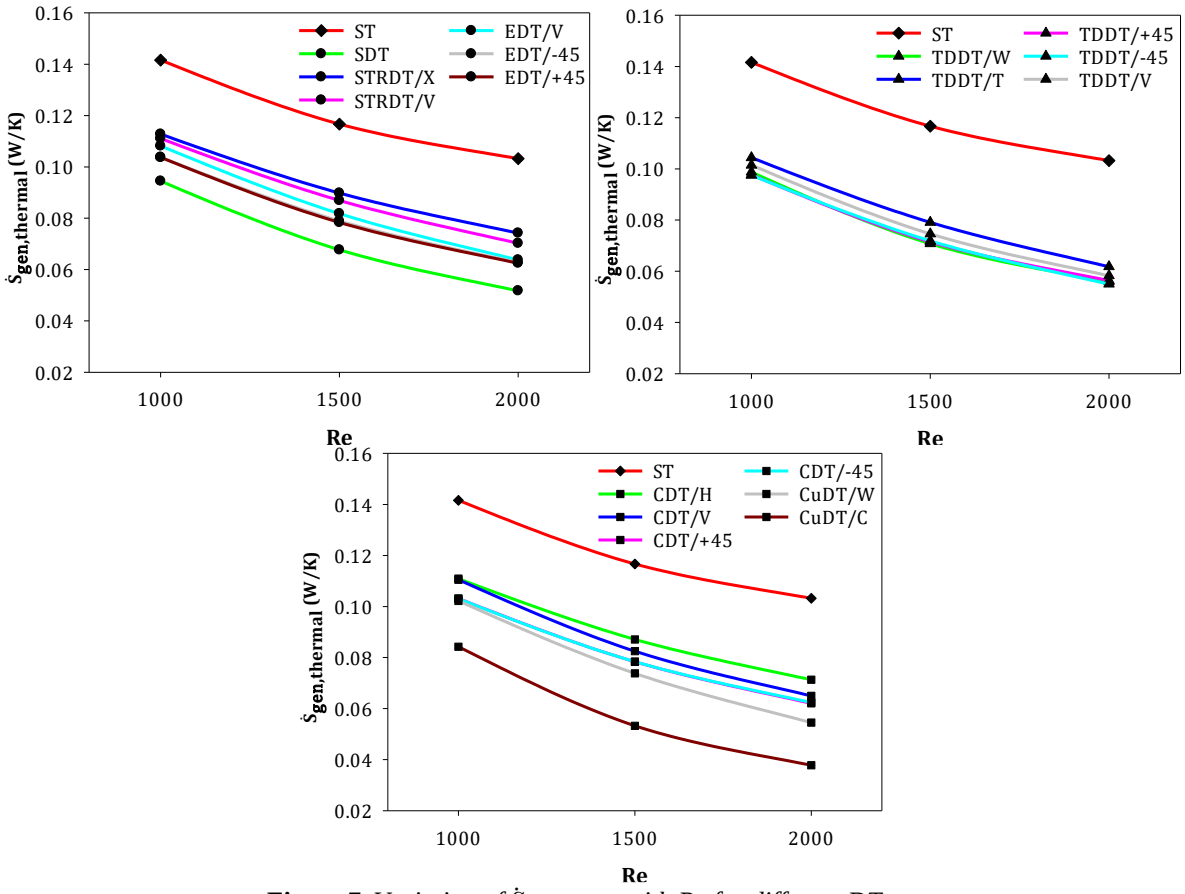

Figure 7. *Variation of $\dot{S}_{gen,\ thermal}$ with Re for different DTs.*

The entropy generation derived from various phenomena such as friction, pressure drop, and viscous dissipation friction are shown in Figure 8. It can be clearly seen that $\dot{S}_{gen,\ frictional}$ of all DTs is greater than that of ST because of the increased surface area and direct impingement of water on the upstream side of the dimpled fins. Among the DTs, CDT/H had the lowest $\dot{S}_{gen,\ frictional}$. The results show that CDT/H has more $\dot{S}_{gen,\ frictional}$ than ST at the rates of 37.35%, 51.37%, and 66.89% for Re=1000, 1500, and 2000, respectively.

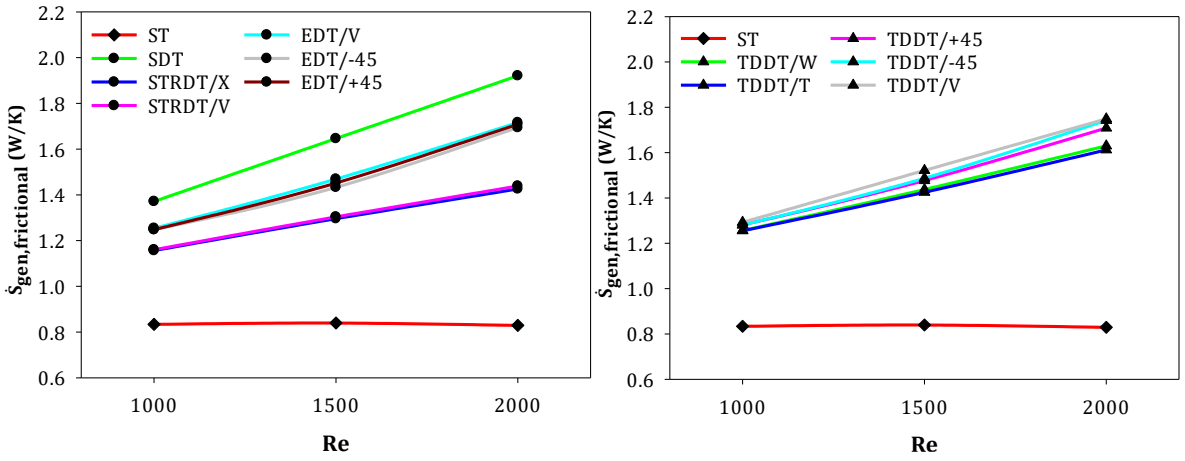

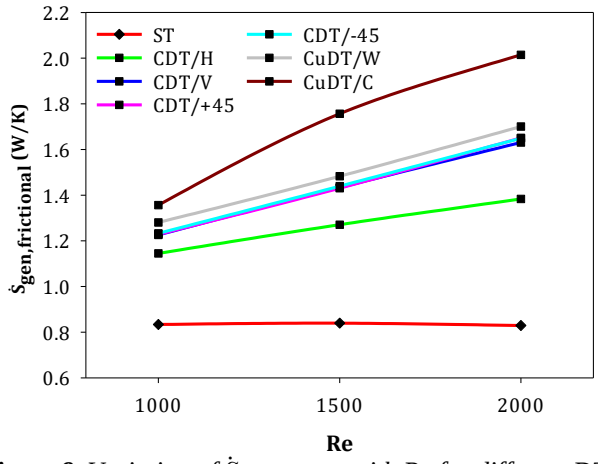

Figure 8. *Variation of $\dot{S}_{gen,\,frictional}$ with Re for different DTs.*

$\dot{S}_{gen,\,total}$ results of DTs are given in Figure 9. According to the results, $\dot{S}_{gen,\,total}$ tends to increment with increasing of Re due to $\dot{S}_{gen,\,frictional}$ is more dominant than $\dot{S}_{gen,\,total}$. CDT/H exhibited the lowest $\dot{S}_{gen,\,total}$ in the scope of this study, as expected. $\dot{S}_{gen,\,total}$ increment rate of CDT/H has been realized as 28.78%, 42.01%, and 56.06% at Re=1000, 1500, and 2000 compared with ST.

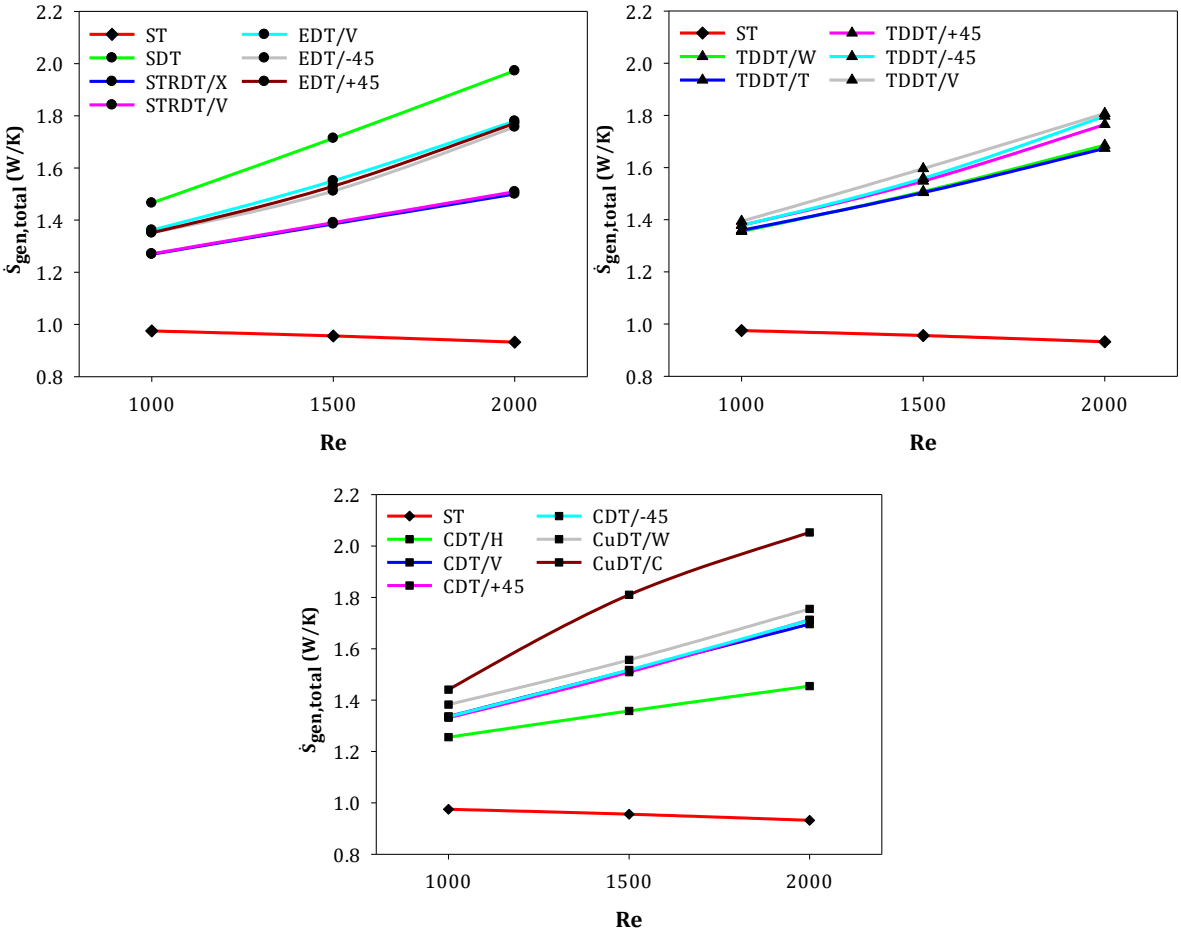

Figure 9. *Variation of $\dot{S}_{gen,\,total}$ with Re for different DTs.*

Evaluation of Be variation of all DTs is shown in Figure 10. The results show that the lowest Be was acquired from CuDT/C because it provided the highest convective heat transfer rate. This result can be explained by the lowest $\dot{S}_{gen,\,thermal}$ achieved by CuDT/C according to the calculations based on Eq. (13).

According to the results, CuDT/C causes 65.94%, 115.96%, and 176.79% less Be than ST for Re=1000, 1500, and 200, respectively.

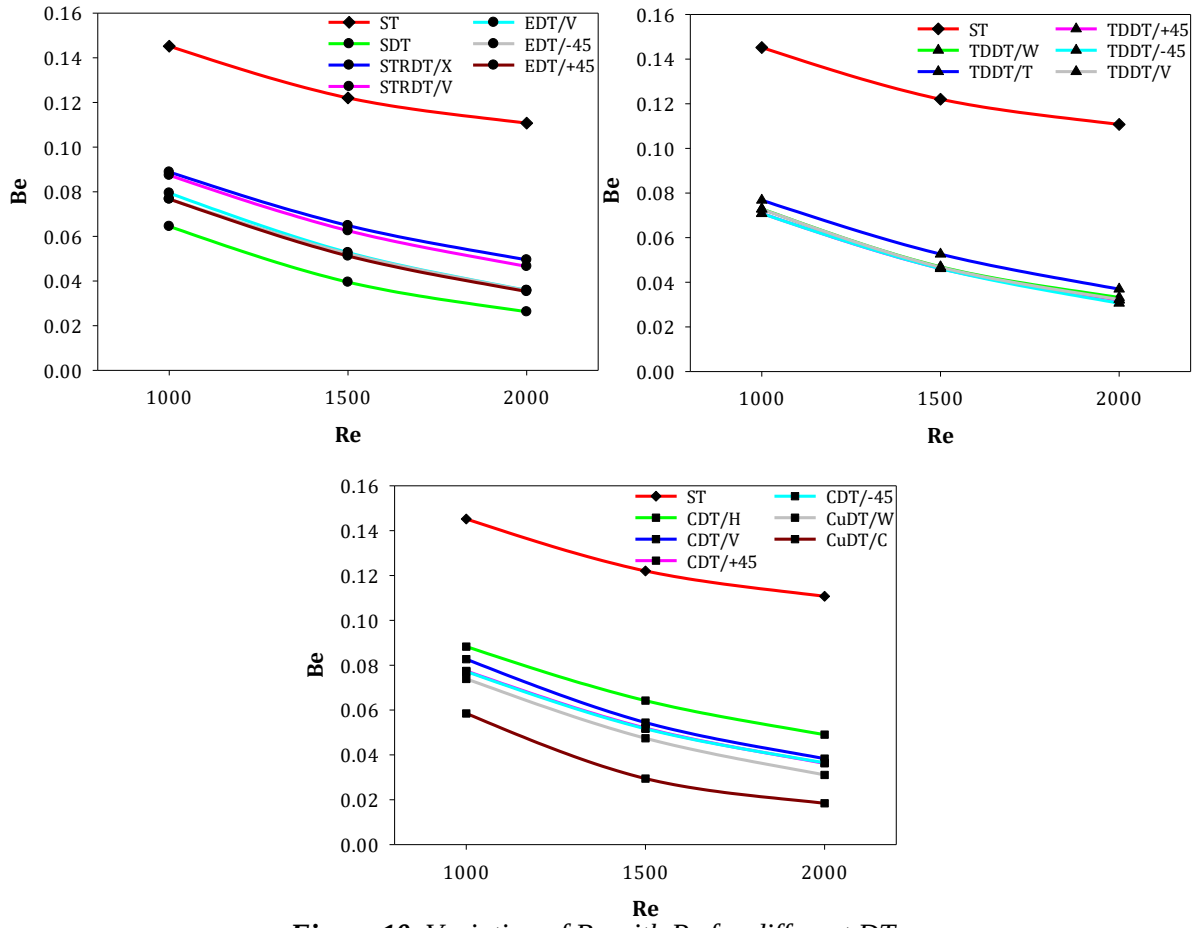

Figure 10. *Variation of Be with Re for different DTs.*

Many figures have been presented below in order to reveal the visual thermo-hydraulic performance of the study. Based on this, local Nu variation of the entire fluid domain is given in Figure 11 for Re=2000. The contours clearly indicate that CuDT/C exhibits a more local Nu enhancement than others because it causes more local severe vortex, especially upstream of the dimpled fins. This rheological behavior is presented and compared in Figure 12 for the entire fluid domain. The velocity vectors given in this figure are given at z=705 mm and Re=2000.

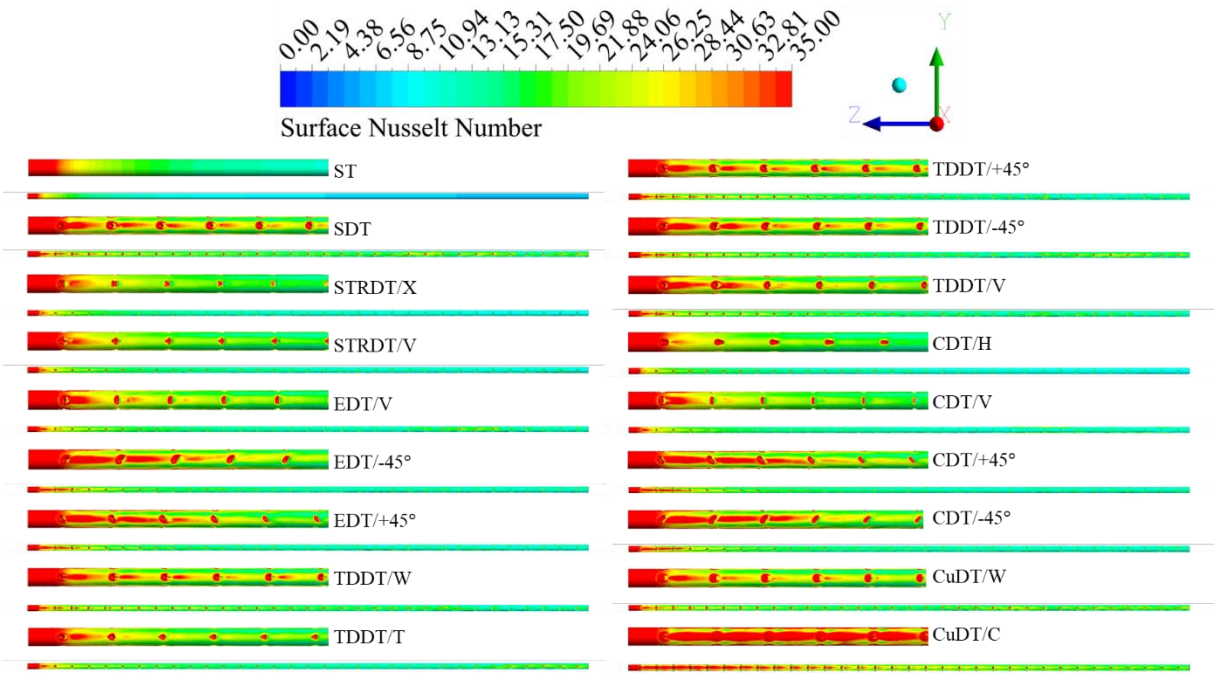

Figure 11. *Visualisation of local Nu variation of the entire fluid domain at Re=2000.*

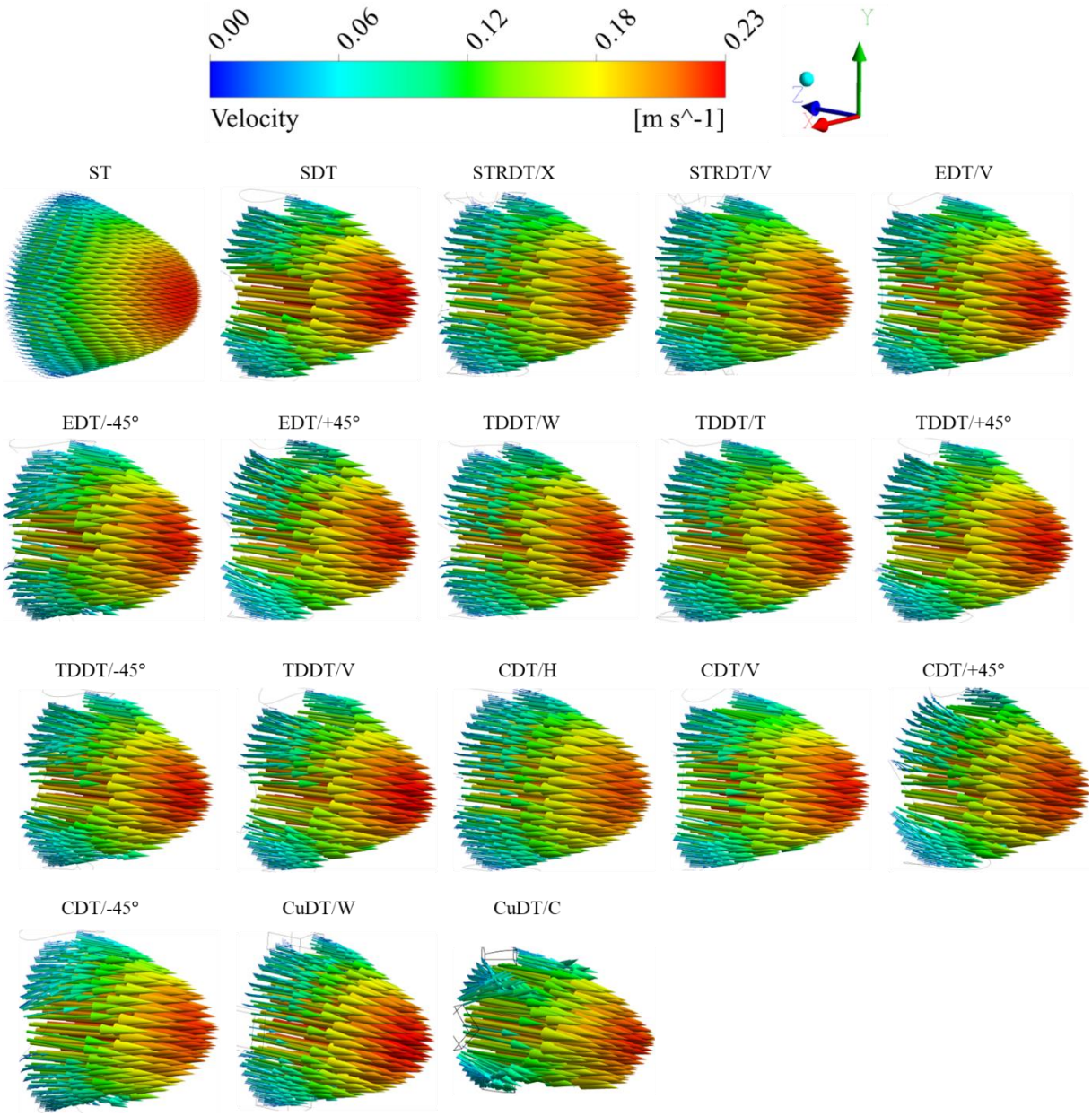

Figure 12. *3D velocity profiles in dimpled fins at z=705 mm and Re=2000.*

On the other hand, the vorticity distribution of DTs is given in Figure 13 for Re=2000. The contours clearly show that the entire dimpled fins formed a vorticity at the upstream side. However, CuDT/C causes a flow behaviour that further increases the vorticity intensity from the upstream side and between the two dimpled fins. Because of this, vorticity distributes both velocity and thermal boundary layers and enhances the convective heat transfer rate. When the differences between the placement angles of the fins are examined, it is seen that CuDT/W causes the same severe vorticity on the upstream side as CuDT/C. However, since CuDT/C causes an increase in vorticity until the subsequent dimpled fin, the convective heat transfer rate is better than CuDT/W.

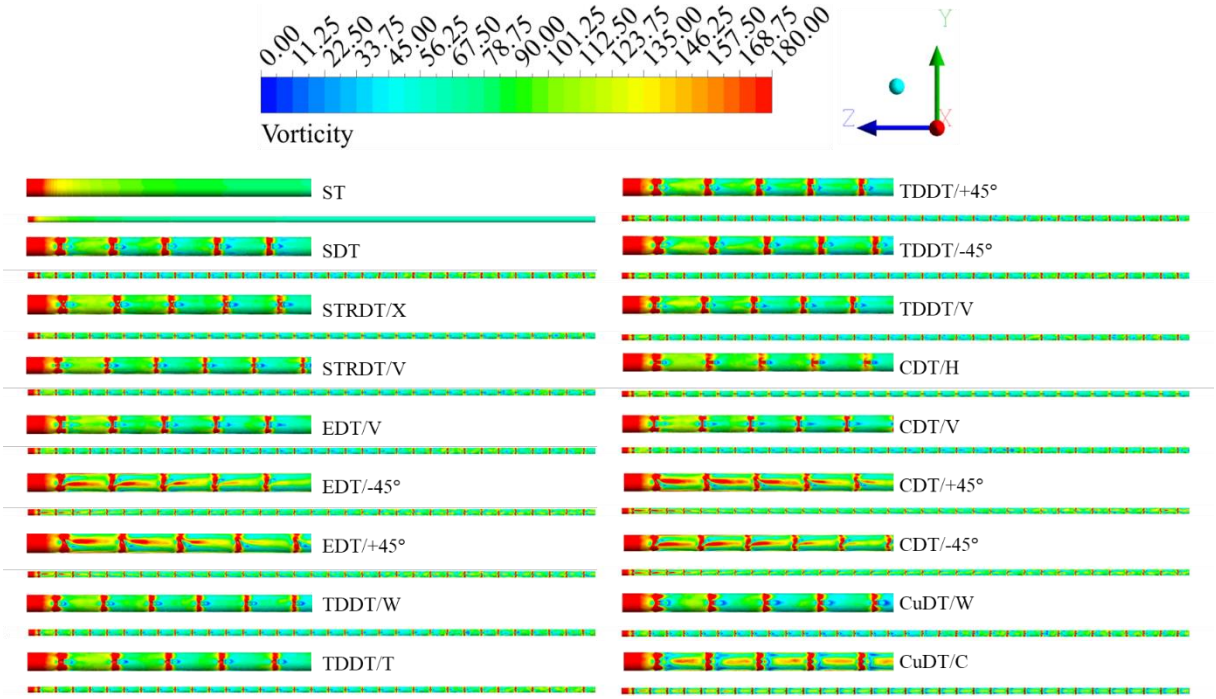

Figure 13. *Vorticity distribution on entire fluid domains at Re=2000.*

The temperature distribution of the fluid domains is presented in Figure 14 for Re=2000. It has been observed from the contours that CuDT/C presents a more homogeneous temperature distribution than others. The underlying factor for this situation is severe vortex dispersion. The heat applied to the tube surface is better transferred to the fluid because of severe vorticities. In this way, the tube surface temperature remains at a lower level and the difference between the wall temperature and bulk temperature given in Eq. (6) tends to decrease. As a result, the convective heat transfer rate increases.

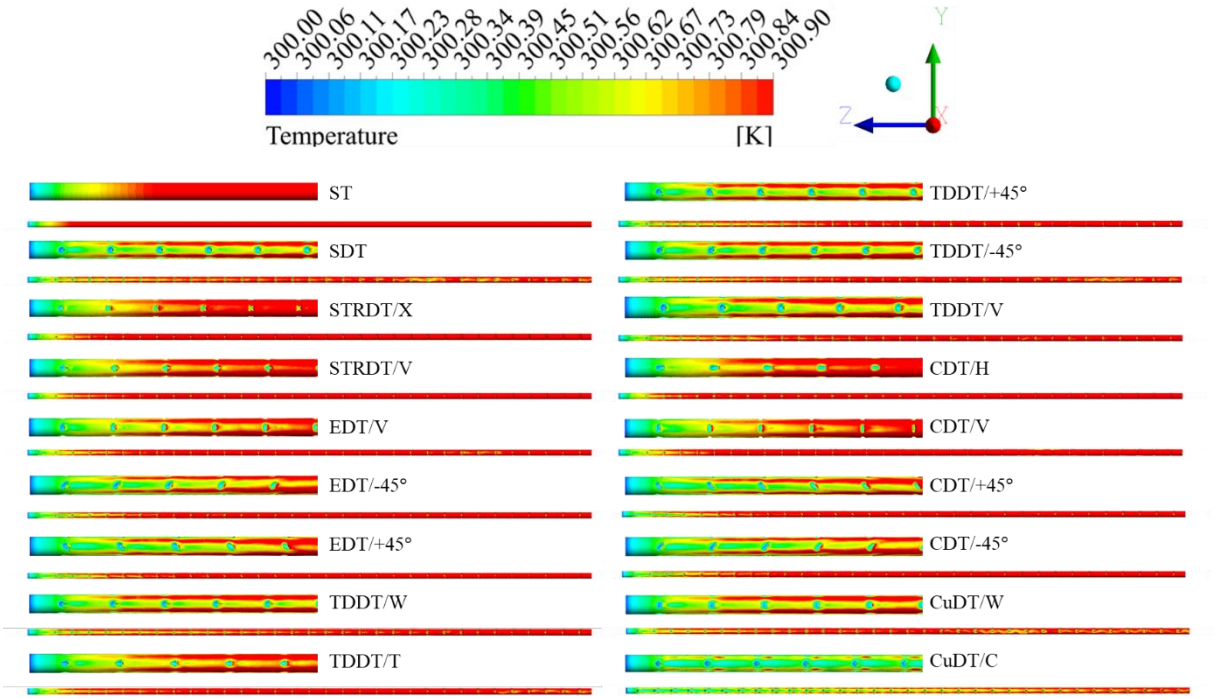

Figure 14. *Temperature distribution over entire fluid domains at Re=2000.*

The pressure drop distribution through the DTs and ST has been given in Figure 15 for Re=2000. It has been clearly seen that a substantial increase is seen in the pressure drops of DTs compared to ST. It has

been determined that the cases that cause the least pressure drop among DTs are STRDT/X, STRDT/X, and CDT/H. It has been determined that the DT causing the highest pressure drop is CuDT/C.

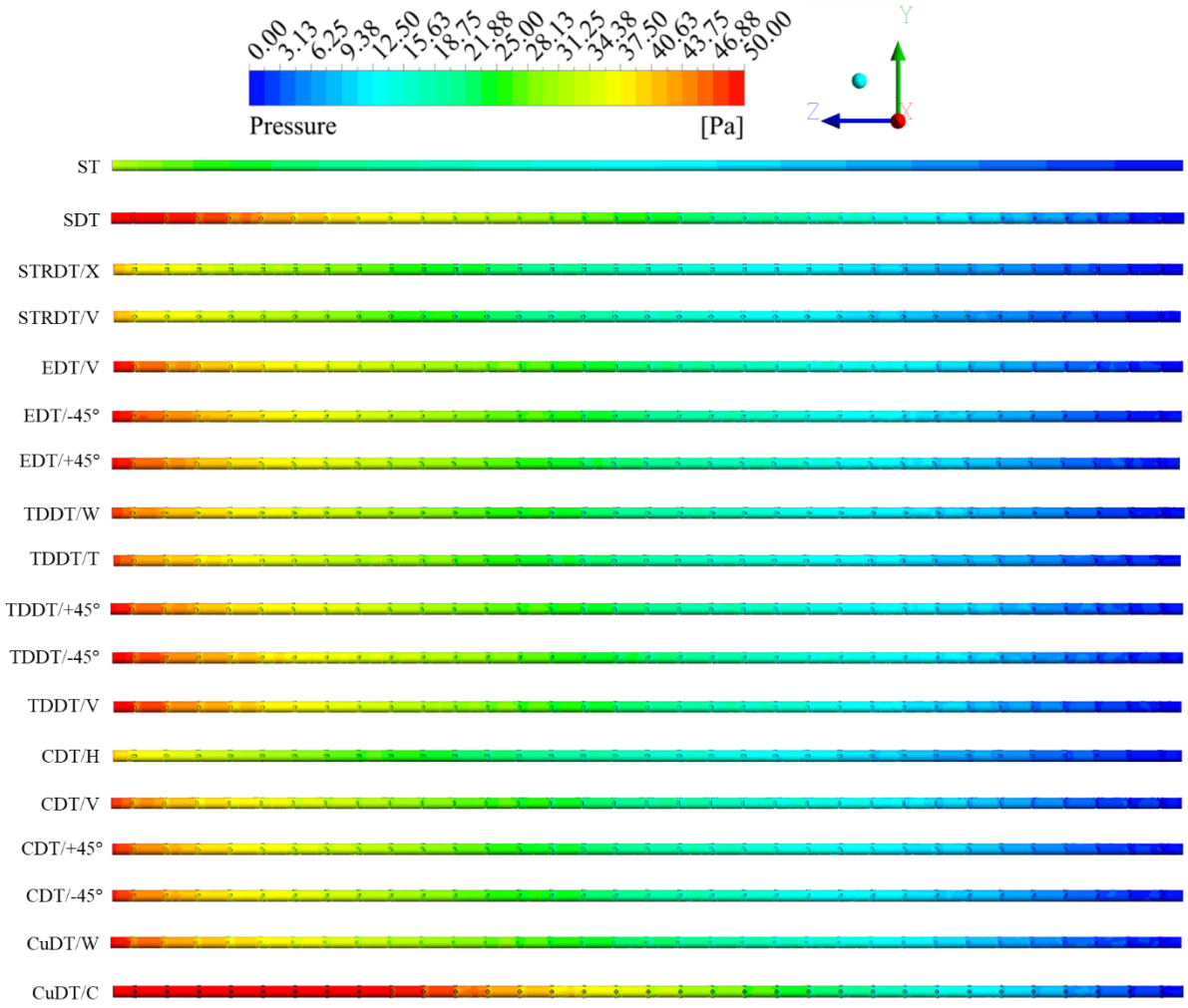

Figure 15. *Pressure drop distribution on entire fluid domains at Re=2000.*

IV. CONCLUSION

Enhancement of the thermo-hydraulic performance of the thermal system is important in terms of reducing fossil fuel consumption and saving. For this reason, researchers and engineers conduct development studies. One of these studies is an enhancement of the thermo-hydraulic performance of heat exchangers, and many studies were conducted under two main groups named as passive and active heat transfer enhancement techniques. In this study, the thermo-hydraulic performance of five dimpled fins aligned, in different directions was, investigated and compared. According to the results, the highest convective heat transfer rate and PEC were exhibited by CuDT/C. In addition, the entropy generation of DTs has been investigated, and the lowest $\dot{S}_{gen,\ total}$ has been acquired by CDT/H.

V. REFERENCES

[1] C. Maradiya, J. Vadher, and R. Agarwal, “The heat transfer enhancement techniques and their Thermal Performance Factor,” Beni-Suef Univ. J. Basic Appl. Sci., vol. 7, no. 1, pp. 1–21, Mar. 2018, doi: 10.1016/J.BJBAS.2017.10.001.

[2] M. H. Mousa, N. Miljkovic, and K. Nawaz, “Review of heat transfer enhancement techniques for single phase flows,” Renew. Sustain. Energy Rev., vol. 137, p. 110566, Mar. 2021, doi: 10.1016/J.RSER.2020.110566.

[3] S. S. Mousavi Ajarostaghi, M. Zaboli, H. Javadi, B. Badenes, and J. F. Urchueguia, “A Review of Recent Passive Heat Transfer Enhancement Methods,” Energies, vol. 15, no. 3, p. 986, Jan. 2022, doi: 10.3390/en15030986.

[4] M. R. Ali et al., “Effect of design parameters on passive control of heat transfer enhancement phenomenon in heat exchangers–A brief review,” Case Stud. Therm. Eng., vol. 43, p. 102674, Mar. 2023, doi: 10.1016/J.CSITE.2022.102674.

[5] H. Lu, M. Xu, L. Gong, X. Duan, and J. C. Chai, “Effects of surface roughness in microchannel with passive heat transfer enhancement structures,” Int. J. Heat Mass Transf., vol. 148, p. 119070, Feb. 2020, doi: 10.1016/J.IJHEATMASSTRANSFER.2019.119070.

[6] S. Paul, N. Lubaba, N. A. Pratik, M. H. Ali, and M. M. Alam, “Computational investigation of cross flow heat exchanger: A study for performance enhancement using spherical dimples on fin surface,” Int. J. Thermofluids, vol. 20, p. 100483, Nov. 2023, doi: 10.1016/J.IJFT.2023.100483.

[7] H. K. Pazarlıoğlu et al., “The first and second law analyses of thermodynamics for CoFe2O4/H2O flow in a sudden expansion tube inserted elliptical dimpled fins,” Int. J. Mech. Sci., vol. 246, p. 108144, May 2023, doi: 10.1016/J.IJMECSCI.2023.108144.

[8] L. Zhang, W. Xiong, J. Zheng, Z. Liang, and S. Xie, “Numerical analysis of heat transfer enhancement and flow characteristics inside cross-combined ellipsoidal dimple tubes,” Case Stud. Therm. Eng., vol. 25, p. 100937, Jun. 2021, doi: 10.1016/J.CSITE.2021.100937.

[9] R. Sabir, M. M. Khan, N. A. Sheikh, and I. U. Ahad, “Effect of dimple pitch on thermal-hydraulic performance of tubes enhanced with ellipsoidal and teardrop dimples,” Case Stud. Therm. Eng., vol. 31, p. 101835, Mar. 2022, doi: 10.1016/J.CSITE.2022.101835.

[10] H. Bucak and F. Yilmaz, “Thermo-hydraulic Performance Investigation of Twisted Tapes Having Teardrop-Shaped Dimple-Protrusion Patterns,” Chem. Eng. Process. - Process Intensif., vol. 168, p. 108593, Nov. 2021, doi: 10.1016/J.CEP.2021.108593.

[11] A. Mironov, S. Isaev, A. Skrypnik, and I. Popov, “Numerical and physical simulation of heat transfer enhancement using oval dimple vortex generators—Review and recommendations,” Energies, vol. 13, no. 20, p. 5243, 2020.

[12] A. Bejan and A. D. Kraus, Heat Transfer Handbook, Volume 1. John Wiley & Sons, Inc., 2003. [Online]. Available: https://books.google.com/books?hl=en&lr=&id=d4cgNG_IUq8C&pgis=1

[13] E. Gürsoy, H. K. Pazarlıoğlu, M. Gürdal, E. Gedik, and K. Arslan, “Entropy generation of ferronanofluid flow in industrially designed bended dimpled tube,” Therm. Sci. Eng. Prog., vol. 37, p. 101620, Jan. 2023, doi: 10.1016/J.TSEP.2022.101620.

[14] E. Gürsoy, E. Çalar, A. Dağdeviren, H. K. Pazarlıoğlu, E. Gedik, and K. Arslan, “Thermo-hydraulic Performance Analysis of Al2O3/water Nanofluid Flow in a Tube Extended by Twisted Tape,” Int. J. Therm. Eng. Mod. Energ., vol. 1, pp. 34–47, 2022, doi: 10.51558/2831-0527.2022.1.1.34.

[15] E. Gürsoy et al., “Effect of magnetic field locations on thermo-magnetic convection performance of Fe3O4/H2O ferrofluid flowing in a novel dimpled tube: An experimental study,” Appl. Therm. Eng., vol. 226, p. 120305, May 2023, doi: 10.1016/J.APPLTHERMALENG.2023.120305.

[16] E. Gürsoy et al., “Energy analysis of magnetite nanofluid flowing in newly designed sudden expansion tube retrofitted with dimpled fin,” Int. J. Heat Mass Transf., vol. 199, p. 123446, Dec. 2022, doi: 10.1016/J.IJHEATMASSTRANSFER.2022.123446.

[17] R. K. Shah and A. L. London, Laminar flow forced convection in ducts: a source book for compact heat exchanger analytical data. Academic press, 2014.

[18] A. F. Mills, “Basic heat and mass transfer,” (No Title), 1999.

[19] Y. A. Çengel and J. M. Cimbala, Fluid Mechanics A Fundamental Approach. 2018.

[20] Y. A. Çengel and A. J. Ghajar, Heat and Mass Transfer Fundamentals & Applications, vol. 59. 2015.